The deformed shape of isotropic and orthotropic plates subjected to bending moments distributed along the edges

M. Gigliotti · M. Minervino

Abstract The paper focuses on the deformation behaviour of isotropic and orthotropic plates subjected to bending moments distributed along the edges, two couples M_0 and $-M_0$ along the longitudinal and the transverse direction, respectively. It can be experimentally noted that the deformed shape of the plate tends to be a saddle for low values of M_0 and cylindrical for high values of M_0. The linear Kirchhoff plate model predicts 'saddle-shaped' deformations for all values of M_0. A model based on energy minimisation and taking into account geometrical nonlinearities is capable to predict the transition from a deformed shape to another: the phenomenon is affected by the plate length-to-width ratio (aspect ratio) and by material anisotropy. These effects are explored throughout the paper.

Keywords Plate deformation · Bending moment · Bifurcation of the solution

This paper is dedicated to the memory of Prof. Piero Villaggio, from the university of Pisa, a Master of Structural Mechanics for many Italian scholars.

M. Gigliotti (✉) · M. Minervino
Département de Physique et Mécanique des Matériaux, Institut Pprime – CNRS – ENSMA – Université de Poitiers, 1, Avenue Clément Ader, 86961 Futuroscope Chasseneuil Cedex, France
e-mail: marco.gigliotti@ensma.fr

1 Introduction

The study of the pure bending of plates is far from being of exclusive academic interest and has many important practical/industrial implications. For instance, bi-metallic plates and disks subjected to uniform temperature differentials [1], unsymmetric composite plates subjected to residual curing stress [2–9] and transient hygrothermal stress [10, 11], composite and hybrid multilayered plates for multifunctional, morphing and smart structural applications [12–20] are all examples of initially flat structures subjected to almost uniform bending load. The mechanical behaviour of some biological structures can be also simulated by employing models of plates under bending [21].

Ashwell [22] has presented an analytical solution for the pure bending of rectangular beams and plates, covering the nonlinear regime and showing that nonlinearities in the bending response are strongly coupled to the development of anticlastic curvature, whose magnitude may be in turn related to the plate length-to-width ratio (aspect ratio, AR) and to the applied bending moment. Some development of the Ashwell solution has been provided by Pao [23] who proposed a simple bending analysis of laminated plates by large-deflection theory, and by Hyer and Bhavani [24], who provided experimental validation to the Ashwell's and Pao's models, for both isotropic and composite plates.

Real structures are rarely subjected to pure simple bending though—in several cases [1–21]—their state of stress can be approximated by a uniform *double*

bending load set; for sample structures—such as the *Timoshenko's bi-metallic strip and of the Hyer's 0/90 unsymmetric composite sample*—a temperature differential promotes a double curvature distortion, whose magnitude depends on the intensity of the heating/cooldown load and on the coefficient of thermal expansion of the elementary lamina [1, 2]: this behaviour can be relatively complex, as curvatures may depend nonlinearly on the applied thermal load and exhibit multistability and bifurcation behaviour.

Experiments on 0/90 composite samples thermally loaded [2] reveal that the plate deformed shape tends to be *saddle-like* (characterised by two curvatures of equal magnitude and opposite sign) and *cylindrical-like*, respectively, for low and high values of the temperature differential: more precisely, starting from a flat configuration, a saddle-like deformed shape develops for low values of the temperature differential while a cylindrical-like deformed shape (whose generator may be along the longitudinal or the transverse direction) takes place starting from a critical value of temperature—more or less well identified experimentally. For high values of the temperature differential in fact two cylindrical-like deformed shapes tend to coexist—one along the longitudinal, another along the transverse direction—separated by a snap-though event: one shape may be reached starting from the other by applying a snapping force. The above reasoning applies for square plates: as far as rectangular plates are concerned multistability can be lost [9] depending on the plate aspect ratio (AR, that is, the plate length-to-width ratio).

The difference between the structural problem of a bi-material structure bent by internal/residual strain/stress (Timoshenko's bi-metallic strip, Hyer's 0/90 unsymmetric composite plate) and that of a plate subjected to a pure double bending moment at its edges and is more apparent than substantial. Of course, the locking of a residual strain/stress field into a bi-material structure will results in multistability at room temperature, while, for plates subjected to bending loads, multiple solutions will vanish as soon as the bending moments are removed. In this sense, the term multistable may sound inappropriate for doubly bent flat plates. However both structural cases may be approximated by a uniform double bending load-set and may exhibit bifurcation behaviour. The existence or the lack of bifurcation behaviour—in both cases—is crucial to the existence of multiple solutions in the bifurcated regime. For the bi-material structure bent by residual strain/stress, an "equivalent" bending moment

can be calculated, so that a full—though approximate—analogy with the flat plate subjected to bending load at the edges can be singled out.

The present paper tries to put forward the nonlinear bending analysis carried out by Ashwell [22], extending it to the case of double bending solicitation and exploring in detail the case of flat square/rectangular isotropic/anisotropic plates subjected to pure double bending moments along the four edges. This analysis *is closer than Ashwell's to structural cases of practical interest* [1–21] but *somehow simpler than many literature models devoted to the simulation/interpretation of complex tests on multistable structures* [12–20, 25, 26] and *aims at investigating conditions for which multistability behaviour can be found*. The applied bending load distributed along the edges of the plate *becomes the main parameter entering the analysis*; like in Ashwell's study [22] the plate materials properties and geometry play a prominent role but—differently from Ashwell—in the present case *they do affect bifurcation behaviour*. To carry out the analysis, two plate theories—both implying plane stress conditions—are taken in consideration (Sect. 2): the first one is based on a classical geometrically linear model (Sect. 2.1), the second one (Sect. 2.2) employs geometrical nonlinearities within the framework of the Von Karman model of plates [27]. In order to find approximate solutions to the latter model, the Rayleigh–Ritz method is employed by the use of two distinct discretized displacement fields: the first one proposed by Hyer in the 1980s [25] for the analogous problem of a 0/90 square unsymmetric composite plate subjected to a temperature differential and involving four unknown coefficients (4-term model), the second one derived from opportune discretization of the analytical in-plane and out-of-plane displacement fields presented by Ashwell [22] and Galletly and Guest [28] and including twelve unknown coefficients (12-term model). In Sect. 3 a comparison between the two models and with a finite element model is provided through simulations involving several specific load cases specialized to isotropic and orthotropic flat plates. Incidentally, the effectiveness of the proposed displacement fields for the analysis of more complex loading conditions (temperature differentials, thermal gradients…) is extrapolated through discussion of the output results. Section 3.3 offers further evaluation of the models by comparison with the Ashwell exact theory [22] for

the nonlinear simple bending of flat plates. For each model, the appropriateness in predicting multistability behaviour, possibly bifurcation behaviour, is tested; moreover the efficiency in terms of computational time is also estimated.

Concluding, the final aim of the paper is twofold:

– to investigate the nonlinear double bending of flat square/rectangular isotropic/anisotropic plates as a sample case for the study of multistable structure (Sects. 3.1, 3.2): in this context the work by Ashwell [22] is put forward and employed (Sect. 3.3) as a support for discussion,
– to investigate the effectiveness of a simple high-order/low-term polynomial approximation for the efficient simulation of this load case, testing its potential ability to be employed for more complex applications.

2 Model approach

2.1 Geometrically linear plate theory

Let us consider an initially flat plate subjected to uniform bending moment distributed along the four edges, $M_{xx} = M_0$ along the x direction, (longitudinal direction) and $M_{yy} = -M_{xx} = -M_0$ along the y direction (transverse direction), see Fig. 1: this scheme can be representative of more complex loading conditions such as those presented in the introductory section, this point will be discussed in Sect. 3.

According to the linear theory of plates (Kirchhoff model, [27]) the longitudinal and transverse in-plane strains, E_{xx} and E_{yy} are given by

$$E_{xx} = E_{xx}^0 - zK_{xx} = \frac{\partial u(x,y)}{\partial x} - z\frac{\partial^2 w(x,y)}{\partial x^2}$$
$$E_{yy} = E_{yy}^0 - zK_{yy} = \frac{\partial v(x,y)}{\partial y} - z\frac{\partial^2 w(x,y)}{\partial y^2} \quad (1)$$

in which E_{xx}^0 and E_{yy}^0 are the membrane longitudinal and transverse in-plane strains, while K_{xx} and K_{yy} are the *longitudinal and the transverse curvatures of the plate*. By Eq. 1 it is noted that E_{xx} and E_{yy} are linear functions of the longitudinal and transverse in-plane displacement fields, $u(x,y)$ and $v(x,y)$, and of $w(x,y)$, which is the out-of-plane displacement field: all fields depend uniquely on x and y. Equation 1 gives also a
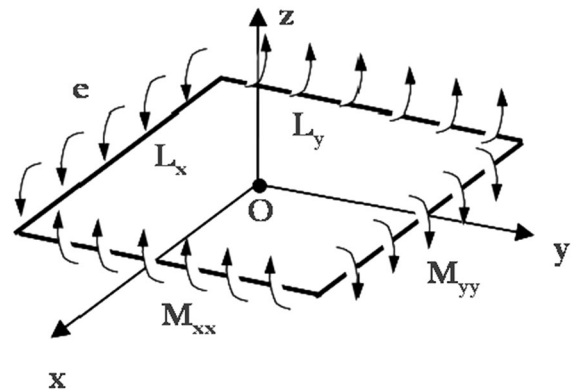

Fig. 1 Geometry of the plate and schematics of the applied bending load

definition of *curvature along a given direction* which is linearly related to $w(x, y)$ and calculated as the second derivative of $w(x, y)$ with respect to that direction. The relations

$$M_{xx} = D(K_{xx} + vK_{yy})$$
$$M_{yy} = D(K_{yy} + vK_{xx}) \quad (2)$$

express the simplest constitutive law for an elastic and isotropic material with bending stiffness D and Poisson ratio v. Taking into account the appropriate boundary conditions, that is:

– the out-of-plane displacement $w(x, y)$ is zero at the centre of the plate,
– the local rotation of the plate along the x and y directions (that is, the first derivative of the out-of-plane displacement with respect to these directions) is zero at the centre of the plate,

under the constraints $M_{xx} = -M_{yy} = M_0$ it allows finding the following explicit expression for the out-of-plane displacement field.

$$w(x, y) = \frac{M_0}{2D(1 - v)}(x^2 - y^2) \quad (3)$$

This result is exact within the limits of the linear theory. According to this model, the in-plane displacements are identically equal to zero while the out-of-plane displacement field is a quadratic function of x and y: this means that the curvature fields are uniform across the plate (they do not depend on x or y), moreover they are of equal magnitude and opposite sign (*saddle-like deformed shape*) for each value of M_0.

This theory fails predicting the behaviour observed through experiments on bi-metallic disks, 0/90 composite plates, multistable morphing plates [1–21] and works only *qualitatively* for low M_0 values: when the out-of-plane displacement becomes higher than the smallest plate dimension (for instance the thickness) the geometrically linear theory must be abandoned.

2.2 Geometrically nonlinear plate theory

According to the simplest geometrically nonlinear plate model [27]—*usually referred as Von Karman plate model*—the in-plane strains are given by

$$E_{xx} = E_{xx}^0 - zK_{xx}$$
$$E_{yy} = E_{yy}^0 - zK_{yy}$$

(4)

with

$$E_{xx}^0 = \frac{\partial u(x,y)}{\partial x} + \frac{1}{2}\left(\frac{\partial w(x,y)}{\partial x}\right)^2$$
$$E_{yy}^0 = \frac{\partial v(x,y)}{\partial y} + \frac{1}{2}\left(\frac{\partial w(x,y)}{\partial y}\right)^2$$

(5)

and

$$K_{xx} = \frac{\partial^2 w(x,y)}{\partial x^2}\bigg/\left(1+\left(\frac{\partial w(x,y)}{\partial x}\right)^2\right)^{3/2} \cong \frac{\partial^2 w(x,y)}{\partial x^2}$$

$$K_{yy} = \frac{\partial^2 w(x,y)}{\partial y^2}\bigg/\left(1+\left(\frac{\partial w(x,y)}{\partial y}\right)^2\right)^{3/2} \cong \frac{\partial^2 w(x,y)}{\partial y^2}$$

(6)

The membrane in-plane strains are related by nonlinear relationships to the out-of-plane displacement function (in-plane/out-of-plane coupling, Eq. 5), while the curvatures defined by Eq. 6 are equivalent to those in Eq. 1 only for moderate rotations, that is, when the square of the local rotation function is everywhere a small number with respect to unity. The total potential energy of the plate, E, can be written down as

$$E = \int_V \frac{1}{2}\mathbf{E}\cdot\mathbb{Q}\mathbf{E}\,dV + E_{ext}$$

(7)

in which $\mathbf{E}$ is the strain tensor, $\mathbf{Q}$ is the plane stress elasticity tensor, V is the volume of the plate ($L_x * L_y * e$) and E_{ext} the potential of the applied external bending moments [27]. The solution of the variational problem

$$\delta E = 0$$

(8)

—asserting that the total potential energy of the plate is stationary at equilibrium—allows finding the unknown displacement field and since nonlinearities are involved by Eqs. 5 and 6, multiple solutions can be found. Stable solutions are those for which

$$\delta^2 E > 0$$

(9)

An exact solution based on Eq. 8 is difficult to find in the general case, even for the specific and relatively simple problem treated here.

The so called Rayleigh–Ritz method can be employed by searching approximate solutions $\mathbf{u}^R(x,y,z)$ of $\mathbf{u}(x,y,z)$ in the sub-space of the q base functions $\chi_i(x,y,z)$ ($i = 1 \ldots q$)

$$\mathbf{u}^R(x,y,z) = \sum_{i=0}^q a_i\chi_i(x,y,z)$$

(10)

a_i are unknown parameters while $\chi_i(x,y,z)$ are a priori chosen base functions (such as polynomial and trigonometric functions, Tchebychev polynomials…) which have to satisfy kinematics boundary conditions only. According to the discretisation in Eq. 10, the total potential energy takes the form

$$E^R\big(\mathbf{u}^R(x,y,z)\big) = E^R(a_i)$$

(11)

therefore Eqs. 8 and 9 become

$$\frac{\partial E^R}{\partial a_i} = 0 \quad i = 1\ldots q \quad \frac{\partial^2 E^R}{\partial a_i\partial a_i} > 0$$

(12)

The problem is thus to find a set of *kinematically admissible displacement field functions* giving a good approximation of the actual displacement fields, satisfying all the kinematics boundary conditions and the compatibility condition.

$$\frac{\partial^2 E_{xx}^0}{\partial y^2} + \frac{\partial^2 E_{yy}^0}{\partial x^2} - 2\frac{\partial^2 E_{xy}^0}{\partial x\partial y} + \left\{\frac{\partial^2 w}{\partial x^2}\frac{\partial^2 w}{\partial y^2} - \left(\frac{\partial^2 w}{\partial x\partial y}\right)^2\right\}$$
$$= 0$$

(13)

The search for appropriate functions is not trivial; recently Vidoli [26] has reported an exhaustive and general study concerning the employment of discrete approximations of the Foppl-von Karman shell model, showing that the intrinsic complexity of the solution for plates subjected to thermal loads requires

simultaneous enrichment of the in-plane and out-of-plane displacement base functions.

A very first choice, proposed by Hyer [25], consists in assuming the out-of-plane function coming from the linear theory (Eq. 3)

$$w^{R4}(x,y) = \frac{1}{2}(ax^2 + by^2) \qquad (14)$$

and deducing the in-plane displacement field functions in such a way that they satisfy the compatibility conditions (Eq. 13)

$$u^{R4}(x,y) = cx - \frac{a^2 x^3}{6} - \frac{abxy^2}{4}$$
$$v^{R4}(x,y) = dy - \frac{b^2 y^3}{6} - \frac{abx^2 y}{4} \qquad (15)$$

Equations 14 and 15 represent the displacement field presented by Hyer [25] for the nonlinear bending of 0/90 unsymmetric plates under thermal solicitations. The model—referred as *4-term model*, the superscript R4 indicating such a discretisation—involves low order polynomial functions for the description of the plate displacements: the out-of-plane functions are polynomials of order two with two unknown terms; the in-plane displacements are polynomials of order three with two additional unknown terms. According to Eq. 6—under the hypothesis of moderate rotations—the longitudinal and transverse curvatures are uniform across the plate and expressed, respectively, by the *a* and *b* coefficients of Eq. 14. In a historical perspective, Hyer's model has been essential for providing a reasonable explanation for the complex multistable behaviour observed in thermally loaded asymmetric composite plates and for predicting their cured shapes and still constitutes a *reference solution* for researchers and scholars approaching the behaviour of smart plates and shells in the nonlinear regime (see the recent review by Herakovich [29] on the matter).

Let us have a qualitative look at the Hyer's solution—initially developed for 0/90 composite plates under temperature differentials—for the case of a plate subjected to double bending moment distributed along the four edges *and see in what this solution differs from the linear one*. The qualitative comparison between the linear and the nonlinear 4-term model can be appreciated in Fig. 2, in which the longitudinal and transverse curvatures—K_{xx} and K_{yy} (corresponding to the *a* and *b* parameters of the
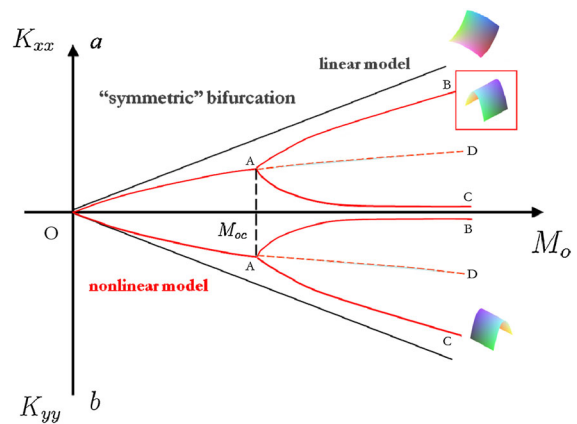
Fig. 2 Schematics evolution of the longitudinal and transverse curvatures as a function of the applied double bending moment (linear and nonlinear models)

nonlinear 4-term model)—are schematically illustrated as functions of the applied bending moment, $M_0 = M_{xx} = -M_{yy}$.

According to Eq. 3, the curvatures calculated by the linear theory are of equal magnitude and opposite sign for all M_0 values, the deformed shape is *saddle-like* across the whole explored loading range, and vary in a linear fashion with respect to M_0. The *a* and *b* curvatures of the nonlinear 4-term model are of equal magnitude and opposite sign up to a critical M_0 value (referred as M_{0c}) so that the *saddle-like* solutions are available along the path O–A: in this range they vary in a nonlinear fashion with respect to the applied bending moment. Beyond M_{0c}, a bifurcation phenomenon takes place giving rise either to a *cylindrical-like shape along the longitudinal direction* (path A–B) either to a *cylindrical-like shape along the transverse direction* (path A–C): the *saddle-like* shape solution is still calculated as an equilibrium solution (dotted line, path A–D) by Eq. 12a which is unlikely to be observed, being unstable according to Eq. 12b. M_{0c} corresponds to a *critical bifurcation* value of M_0 for which the following explicit expression can be given

$$M_{oc} = \frac{Ee^3}{1 - v^2}\sqrt{\frac{20}{3}\frac{1 + v}{2L_x^4}} \qquad (16)$$

Equation 16 is valid within the framework of the nonlinear 4-term model approximation, for a square plate with side L_x made of isotropic material and indicates that the main parameters affecting M_{0c} are the material properties (Young's modulus and Poisson's ratio), the thickness of the plate and its length.

The nonlinear 4-term model captures bifurcation behaviour also for rectangular plates: in this case—for an isotropic plate with length L_x and width L_y—the critical bending moment is given by

$$M_{oc} = \frac{Ee^3}{1-v^2} \sqrt{\frac{20}{3} \frac{1+v}{L_x^4 + L_y^4}} \tag{17}$$

Equation 17 predicts that the critical bending moment is slightly affected by the plate AR. Since the nonlinear solution derives from a numerical calculation, the critical value of the applied bending moment, M_{0c}, for both square and rectangular plates (Eqs. 16 and 17) is approximate and depends on the chosen level of discretisation.

The presented bifurcation behaviour—for both square and rectangular plates—can be referred as *symmetric bifurcation*, since it exhibits the same features along both the longitudinal and the transverse direction: symmetric bifurcation reproduces an abstract behaviour which can be never observed in practice, due to structural, geometrical, material, load imperfections. Moreover, within the framework of bi-material plates and shells subjected to temperature differentials, experimental evidence of bifurcation behaviour has been reported for square configurations but not for rectangular ones [2, 9].

The following section will be devoted to finding an answer to the question: *is a simultaneous enrichment of the assumed in-plane and out-of-plane displacement functions capable to enhance the predictions of the 4-term model, in particular for what concerns the range of existence of multistable solutions, for both square and rectangular plates?* In order to increase the solution, the following reasoning will be applied:

– the out-of-plane approximate displacement function, $w(x, y)$, will be generated by proper development (and truncation) of the Ashwell's analytical solution [22] for the nonlinear pure bending of isotropic plates,
– the in-plane approximate displacement functions, $u(x, y)$ and $v(x, y)$ will be developed by applying an analogous procedure to the semi-analytical solution proposed by Galletly and Guest [28] for the bending of composite slit tubes.

Ashwell found that—for a flat plate bent along the longitudinal direction, x, with given radius of curvature, R—the exact out-of-plane displacement of a central transverse section of the plate ($x = 0$) is given by

$$\frac{w(y)}{e} = \left[B\cosh\left[\alpha L_y\left(\frac{y}{L_y}\right)\right] \cos\left[\alpha L_y\left(\frac{y}{L_y}\right)\right] \right. \\ \left. + C\sinh\left[\alpha L_y\left(\frac{y}{L_y}\right)\right] \sin\left[\alpha L_y\left(\frac{y}{L_y}\right)\right] \right] \tag{18}$$

with

$$B = \frac{v}{\sqrt{3(1-v^2)}} \frac{\sinh\left(\frac{\alpha L_y}{2}\right)\cos\left(\frac{\alpha L_y}{2}\right) - \cosh\left(\frac{\alpha L_y}{2}\right)\sin\left(\frac{\alpha L_y}{2}\right)}{\sinh(\alpha L_y) + \sin(\alpha L_y)} \tag{19}$$

$$C = \frac{v}{\sqrt{3(1-v^2)}} \frac{\sinh\left(\frac{\alpha L_y}{2}\right)\cos\left(\frac{\alpha L_y}{2}\right) + \cosh\left(\frac{\alpha L_y}{2}\right)\sin\left(\frac{\alpha L_y}{2}\right)}{\sinh(\alpha L_y) + \sin(\alpha L_y)} \tag{20}$$

and

$$\alpha L_y = \sqrt[4]{3(1-v^2)}\frac{L_y}{Re} \tag{21}$$

The adimensional parameter $\tau = \frac{L_y^2}{Re}$ is important for determining the mode of distortion: for low values of τ the plate can develop anticlastic curvature ('linear' or 'beam behaviour'), for high values of τ the anticlastic curvature is constrained and the plate remains substantially flat except near the edge ('large plate behaviour'). It is reasonable to develop the trigonometric functions appearing in Eq. 1 in Taylor's series up to a desired order, that is

$$\sin x = \sum_{n=0}^{\infty} \frac{(-1)^n}{(2n+1)!} x^{2n+1} \tag{22}$$

$$\cos x = \sum_{n=0}^{\infty} \frac{(-1)^n}{(2n)!} x^{2n} \tag{23}$$

$$\sinh x = \sum_{n=0}^{\infty} \frac{1}{(2n+1)!} x^{2n+1} \tag{24}$$

$$\cosh x = \sum_{n=0}^{\infty} \frac{1}{(2n)!} x^{2n} \tag{25}$$

For instance, stopping the series (Eqs. 22–25) at $n = 1$ gives

$$B = -\frac{q}{24}(\alpha L_y)^2 \tag{26}$$

$$C = \frac{q}{2}\left[1 - \frac{1}{12}\left(\frac{\alpha L_y}{2}\right)^4\right] \qquad (27)$$

$$\frac{w(y)}{e} = C_0 + C_1 y^2 + C_2 y^4 - C_3 y^6 \qquad (28)$$

with

$$C_0 = -\frac{q\mu}{24}\frac{L_y^2}{Re} \qquad (29)$$

$$C_1 = \left(\frac{q\mu}{2eR} - \frac{q\mu^3 L_y^4}{384 e^3 R^3}\right) \qquad (30)$$

$$C_2 = \frac{q\mu^3}{96}\frac{L_y^2}{e^3 R^3} \qquad (31)$$

$$C_3 = \left(\frac{q\mu^3}{72 e^3 R^3} - \frac{q\mu^5 L_y^4}{13824 e^5 R^5}\right) \qquad (32)$$

in which μ and q depend only upon the material properties

$$\mu = \sqrt{3(1 - v^2)} \qquad (33)$$

$$q = \frac{v}{\sqrt{3(1 - v^2)}} \qquad (34)$$

The polynomial approximation of the Ashwell exact solution, Eq. 28, can be expanded in order to take into account the dependency upon the x coordinate, namely

$$w^{R12}(x,y) = c_1 x^2 + c_2 y^2 + c_3 x^4 + c_4 y^4 + c_5 x^6 + c_5 y^6 \qquad (35)$$

In Eq. 35 the coefficients C_0, C_1, C_2, C_3 of Eq. 28 are replaced by 6 unknown terms, c_1–c_6. Since the plate is clamped at its centre ($x = 0$, $y = 0$) the C_0 terms can be setup to zero without loosing generality. Equation 35 does not take into account mixed terms related to the product xy, the relevance of this approximation will be discussed next.

The in-plane displacement fields can be formulated following a similar procedure employing the semi-analytical displacement fields proposed by Galletly and Guest [28] for the distortion of composite slit tubes under bending. When the plate has a doubled curved deformed shape, with longitudinal curvature K_{xx}, a distorted section appears schematically as illustrated in Fig. 3.
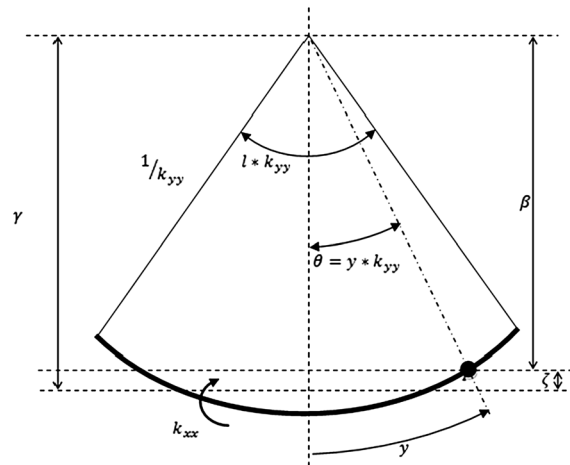
Fig. 3 Schematics of a section distortion in the case of a plate subjected to double bending moment (the scheme follows Ref. [28])

The parameter γ represents the distance between the neutral axis of the section and the center of bending, the strain along the x direction has a linear dependence from the location of the neutral axis. Indeed, considering a constant deformation on the neutral plane E_x, the in-plane strain E_{xx}^0 is given by

$$E_{xx}^0 = E_x - \varsigma K_{xx} \qquad (36)$$

where ζ represents the displacement from the neutral axis, which can be expressed as (with the symbols in Fig. 1)

$$\varsigma = \gamma - \beta = \frac{1}{K_{yy}}\frac{2\sin\left(\frac{L_y K_{yy}}{2}\right)}{L_y K_{yy}} - \frac{1}{K_{yy}}\cos\left(y K_{yy}\right) \qquad (37)$$

The in-plane strain has therefore the form

$$E_{xx}^0 = E_x - K_{xx}\left[\frac{1}{K_{yy}}\frac{2\sin\left(\frac{L_y K_{yy}}{2}\right)}{L_y K_{yy}} - \frac{1}{K_{yy}}\cos\left(y K_{yy}\right)\right] \qquad (38)$$

The trigonometric function can be again developed in Taylor series and stopping the development for $n = 2$, the in-plane strain becomes

$$E_{xx}^0 = E_x + K_{xx}\left[\frac{K_{yy}}{2}\left(\frac{L_y^2}{12} - \frac{K_{yy}^2 L_y^4}{960} - y^2 + \frac{K_{yy}^2}{12}y^4\right)\right] \qquad (39)$$

and—using a set of independents coefficients.

$$E_{xx}^0 = c_7 + c_9 y^2 + c_{11} y^4 \tag{40}$$

The in-plane strain along the y direction, E_{yy}^0, can be found by following a similar procedure, thus giving

$$E_{yy}^0 = c_8 + c_{10} x^2 + c_{12} x^4 \tag{41}$$

The in-plane displacements can be obtained by integration of the strain fields

$$u(x, y) = \int \left[E_{xx}^0 - \frac{1}{2} \left(\frac{\partial w}{\partial x} \right)^2 \right] dx \tag{42}$$

$$v(x, y) = \int \left[E_{yy}^o - \frac{1}{2} \left(\frac{\partial w}{\partial y} \right)^2 \right] dy \tag{43}$$

The final form of the displacement field functions in given by Eqs. 35, 44 and 45.

$$
\begin{aligned}
u^{R12}(x, y) = {} & c_7 x - \frac{2}{3} c_1^2 x^3 - \frac{8}{5} c_1 c_3 x^5 - \frac{8}{7} c_3^2 x^7 \\
& - \frac{12}{7} c_1 c_5 x^7 - \frac{8}{3} c_3 c_5 x^9 - \frac{18}{11} c_5^2 x^{11} \\
& + c_9 x y^2 + c_{11} x y^4
\end{aligned} \tag{44}
$$

$$
\begin{aligned}
v^{R12}(x, y) = {} & c_8 y - \frac{2}{3} c_2^2 y^3 - \frac{8}{5} c_2 c_4 y^5 - \frac{8}{7} c_4^2 y^7 \\
& - \frac{12}{7} c_2 c_6 y^7 - \frac{8}{3} c_4 c_6 y^9 - \frac{18}{11} c_6^2 y^{11} \\
& + c_{10} x^2 y + c_{12} x^4 y
\end{aligned} \tag{45}
$$

This model involves 12 independent parameters, c_1–c_{12} and is referred as *12-term model*, the superscript R12 indicating such a discretisation. The minimizing of the total potential energy (Eqs. 8–9) gives a system of 12 nonlinear equations whose unknowns are the coefficients c_i.

3 Simulations

In this Section the geometrically nonlinear 12-term model developed and presented in Sect. 2 is compared to the Hyer's 4-term model [25] through the analysis of three different case studies: depending on the application comparison with the linear theory, the finite element model and the analytical model by Ashwell [22] is also provided. The presentation of results is organised in three distinct sections, namely:

– Section 3.1, which is the heart of the discussion, is concerned with the nonlinear double bending of square and rectangular isotropic plates. The 12-term model is compared to the 4-term model, the linear theory and the finite element model,

– Section 3.2 is concerned with the nonlinear double bending of square and rectangular orthotropic plates and compares the 12-term and the 4-term models,

– Section 3.3 focuses on the nonlinear simple bending of isotropic square and rectangular plates. Here the 12-term and the 4-term model are both compared to the analytical model by Ashwell [22].

3.1 Isotropic square and rectangular plates under nonlinear double bending

The multistable behaviour of a freestanding isotropic plate under nonlinear double bending is explored by comparing the 12-term and the 4-term models. Since an analytic exact solution for this problem does not exist further comparison to a finite element model is provided; for reference, the results of the linear model simulations are also given. The *average* longitudinal and the transverse curvatures calculated by the three models are illustrated as functions of the applied bending moment ($M_{xx} = -M_{yy} = M_0$); moreover the out-of-plane displacement fields along given directions are given as output. Material properties are given in Table 1.

While the predictions of the linear theory are found by simply inverting Eq. 2, the curvatures of the 4-term nonlinear model are given by the parameters a and b in Eqs. 14 and 15, which are calculated by solving Eq. 12 numerically by means of a MATLAB solver: according to the 4-term model, the curvatures are uniform across the plate. The calculation of the curvatures predicted by the 12-term model needs some post-processing: in this case the twelve unknown parameters c_1-c_{12} characterising the displacement field functions, Eqs. 35, 44 and 45 are first calculated numerically by a dedicated Netwon–Raphson solver implemented in the MATLAB code then the local curvatures (depending on x and y) calculated by means of Eq. 6, under the hypothesis of moderate rotation. Finite element model calculations have been performed by employing the ABAQUS commercial

Table 1 Isotropic material properties for the numerical simple bending simulations

E (GPa)	v_{12}
70	0.33

software and by modelling both square and rectangular plate with "S4" 4-node doubly curved thin shell elements, each element being characterised by a plane 2 mm × 2 mm surface. The bending load has been applied at the surface edges through the "shell edge load" option allowing distributing uniformly the solicitation; by adopting a purely elastic material behaviour, a simple 1-step static analysis has been carried out, taking into account the large displacement/moderate rotation effects through the NLGEOM option. The main difficulty with the finite element model is that the user has to "drive" the solver in the presence of multiple solutions or in order to follow bifurcated branches; by default the finite element model has the tendency to follows unique branches even when they become eventually unstable after crossing a bifurcation point. In this case, in order to find alternative stable solutions or to promote "switching" between two adjacent stable solutions, some kind of asymmetry has to be introduced into the model, for instance by reproducing a rather small artificial geometrical imperfection or by integrating some modest perturbation load at some convenient location of the structure; in the present work a concentred force of magnitude ± 1 N has been applied at the upper-right plate coin to allow the plate "snapping" from one stable configuration to an adjacent one (exhibiting almost the same energetic content); this load has been removed in an extra step in order to avoid excessive perturbation of the numerical solution.

In order to compare the 12-term and the finite element model (predicting nonuniform curvature distortion) to the linear and the 4-term models the curvatures K_{xx} and K_{yy} have been *averaged* by employing the following formula

$$K_{xx} = \frac{1}{L_x} \int_{-\frac{L_x}{2}}^{\frac{L_x}{2}} \left(\frac{\partial^2 w}{\partial x^2} \right)_{y=0} dx \qquad (46)$$

$$K_{yy} = \frac{1}{L_y} \int_{-\frac{L_y}{2}}^{\frac{L_y}{2}} \left(\frac{\partial^2 w}{\partial y^2} \right)_{x=0} dy \qquad (47)$$

The material properties employed for simulations are summarised in Tab. 1.

Figure 4a illustrates the longitudinal and the transverse average curvatures as a function of M_0 for a square isotropic plate (AR = 1), as predicted by the linear (dotted line), the 4-term (cross points), the 12-term (circles) and the finite element (continuous line) models.

The nonlinear models behave all qualitatively as illustrated schematically in Fig. 2 differing in a substantial way from the predictions of the linear theory. While the curvatures calculated by the linear model are of equal magnitude and opposite sign (saddle-like deformed shape), for each value of the applied bending moment and depend linearly on M_0, the 4-term, the 12-term and the finite element nonlinear models predict symmetric bifurcation behaviour, though differing slightly from a quantitative point of view.

Discrepancies reside above all in the prediction of the critical bending moment, M_{0c}, the value predicted by the 12-term nonlinear model for a square isotropic plate, that is

$$M_{oc} = \frac{Ee^3}{1 - v^2} \sqrt{15.5 \frac{1 + v}{2L_x^4}} \qquad (48)$$

differs slightly from the equivalent value given by the 4-term model, Eq. 16. While the discrepancy resides in the different level of discretisation characterising the two models, the exactness of the two expressions cannot be checked since an explicit solution for this problem does not exist. Taking as 1 the values calculated by the 4-term nonlinear model, Table 2 gives a comparison among the various models in the prediction of the critical bending moment values. Furthermore, Fig. 4b illustrates the adimensional out-of-plane displacements (w/e) calculated along the longitudinal (x/L_x) and transverse (y/L_y) coordinates, respectively at $y = 0$ and at $x = 0$, for several values of the applied bending moment. Looking at the illustration of Fig. 4 and reading through the numerical results in Table 2, the comparison with finite element simulations does not help deciding in favour of one of the two approximated displacement fields, at least for square plates (AR = 1): from one side the average curvatures predicted by the finite element model look globally closer to the 12-term displacement model, from another side as soon as the calculation of the critical bending moment is concerned, the 4-term model gives predictions which are in good agreement with the finite element model. It must be emphasized that the finite element model—though sufficiently refined—by no means can be
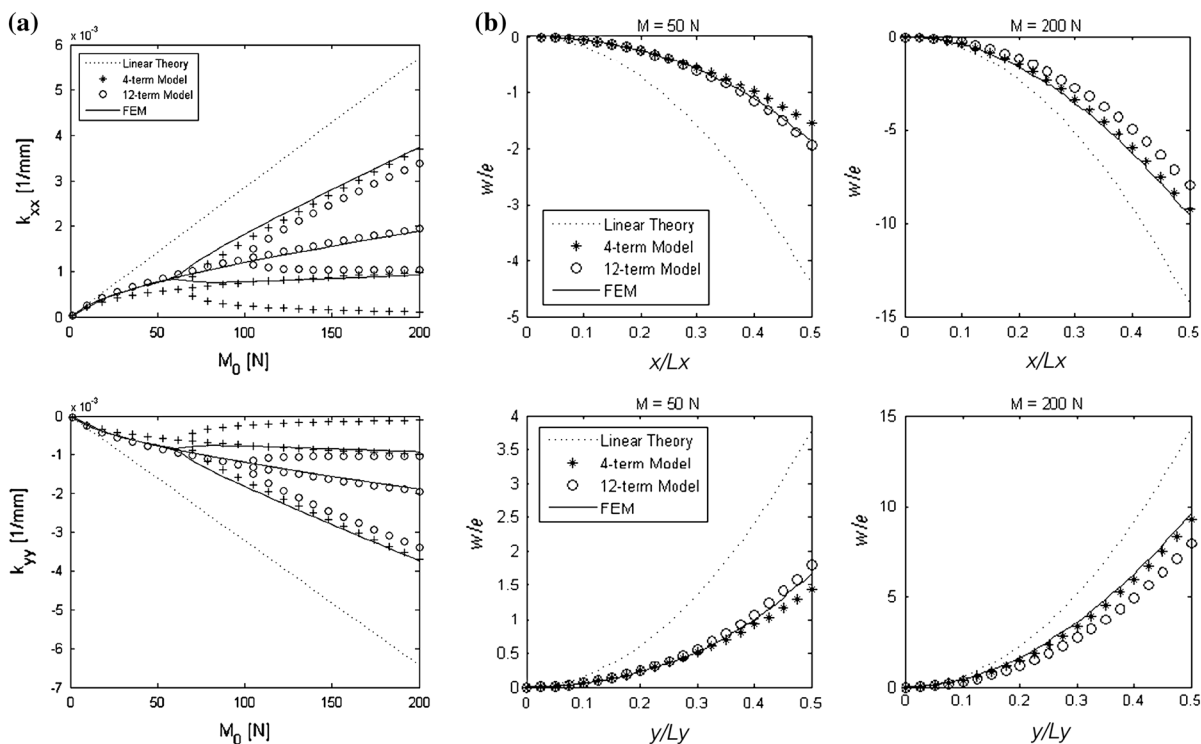
Fig. 4 a Longitudinal and transverse curvatures and **b** out-of-plane displacement as a function of the adimensional longitudinal (x/L_x) and transverse (y/L_y) coordinate for several values of the applied double bending moment ($M_{xx} = -M_{yy} = M_0$) for a square isotropic plate (AR = 1)

considered as an exact/reference solution, since its predictions depend on the adopted numerical spatial/temporal discretisation; this reasoning applies to the case of square plates (AR = 1), for which the calculation of the bifurcated branches (and of the bifurcation point) relies on the artificial procedure employed to catch bifurcation.

Figure 5 illustrates the *average* curvatures as a function of M_0 for a rectangular isotropic plate (AR = 2), as predicted by the linear (dotted line), the 4-term (cross points), the 12-term (circles) and the finite element (continuous line) models.
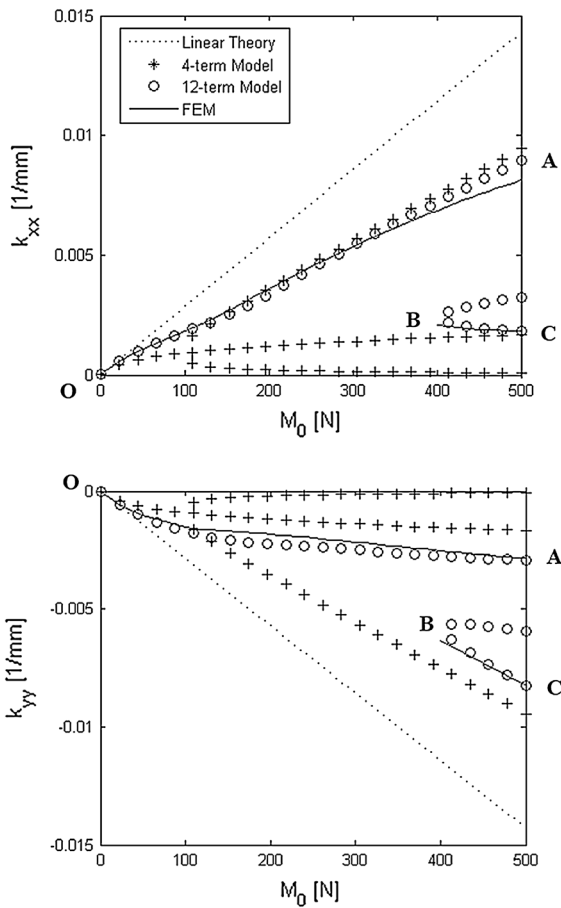
The 4-term model keeps predicting symmetric bifurcation behaviour, the calculated critical bending moment (Eq. 17) differing only slightly from that given by Eq. 16 for a square plate (AR = 1). *The 12-term and the final element model predict a completely different behaviour:* by increasing M_0 a unique cylindrical-like shape along the longitudinal direction has the tendency to develop (path O–A), while an alternative quasi cylindrical shape—along the transverse direction—becomes available at some point

(path B–C). Unstable solutions are not plotted for both the 12-term *and* the finite element model. Figure 5 brings an important conclusion about the multistable behaviour of rectangular (but not narrow) rectangular plates subjected to (symmetric) double bending load: *though multiple stable equilibrium shapes can be effectively observed, the transition takes place without classical bifurcation* (point B *is not a classical bifurcation point*), *leading to a response behaviour which is not symmetric.* This time the finite element predictions are in support of the 12-term model, the agreement between the two solutions is excellent in almost all the explored loading range.

Figure 6a illustrates the *average* curvatures as a function of M_0 for a rectangular isotropic *narrow* plate (AR = 10), as predicted by the linear (dotted line), the

Table 2 Critical bending moment for a square isotropic plate

	4-term	12-term	FEM
M_{0c} [N]	1	1,54	0,87

Fig. 5 Longitudinal and transverse curvatures as a function of the applied double bending moment ($M_{xx} = -M_{yy} = M_0$) for a rectangular isotropic plate (AR = 2)

4-term (cross points), the 12-term (circles) and the finite element (continuous line) models.

Still for narrow strips, the 4-term model keeps predicting symmetric bifurcation behaviour, whose value of critical bending moment differs only slightly from that predicted for square and moderately rectangular plates. The 12-term *and* the finite element model both predict a distinctly different behaviour, *calculating—in all the explored loading range—a unique saddle-like shape developing along path O–A with increasing M_0: moreover, this solution is reasonably close to that predicted by the linear model, for almost all values of bending loading in explored range.* Figure 6b—illustrating the adimensional out-of-plane displacements (w/e) calculated along the longitudinal (x/L_x) and transverse (y/L_y) coordinates, respectively at $y = 0$ and at $x = 0$, for several values of the applied

bending moment—strengthens the conviction that the 12-term and the finite element model *are predicting the solution with almost the same level of accuracy and are both very close to the linear solution.*

In conclusion while some reserve can be expressed concerning the ability of the 12-term nonlinear model to predict *exactly* (or it should be said "more exactly than" the 4-term model) the behaviour of square plates (AR = 1), *the qualitative and quantitative accuracy gained thanks to the employment of the 12-term model for the simulation of moderately and narrow rectangular plates is evident*: this is due to the capability of the refined solution to catch the loss of classical symmetric bifurcation and of multistability phenomena which take place *as soon as the geometrical symmetry of the configuration is broken* due to a change in the plate geometrical arrangement (passing from square to rectangular): this aspect will be discussed in more detail in Sect. 3.3.

To conclude this section, it could be demonstrated that a refined out-of-plane displacement field of the form

$$w^{R15}(x, y) = c_1x^2 + c_2y^2 + c_3x^4 + c_4y^4 + c_5x^6 + c_6y^6 \\ + c_{13}x^2y^2 + c_{14}x^4y^2 + c_{15}x^2y^4$$

(49)

taking into account 15 unknown parameters and making use of mixed terms (xy cross products), do not enhance significantly the exactness of solution, leading to a maximal discrepancy of around 3 % and increasing the computational cost of the numerical solution of around three times with respect to the 12-term model.

3.2 Orthotropic square and rectangular plates under nonlinear double bending

This Section is devoted to the prediction of the behaviour of orthotropic square and rectangular plates subjected to bending moments applied at the four edges ($M_{xx} = -M_{yy} = M_0$). Material properties for the orthotropic ply are reported in Table 3. The analysis—supported by the conclusions of Sect. 3.1—relies on the conviction that the 12-term model is more prone to catch the loss of classical bifurcation and multistability phenomena taking place in structural configurations subjected to the breaking of some sort of symmetry—geometrical, for plates whose
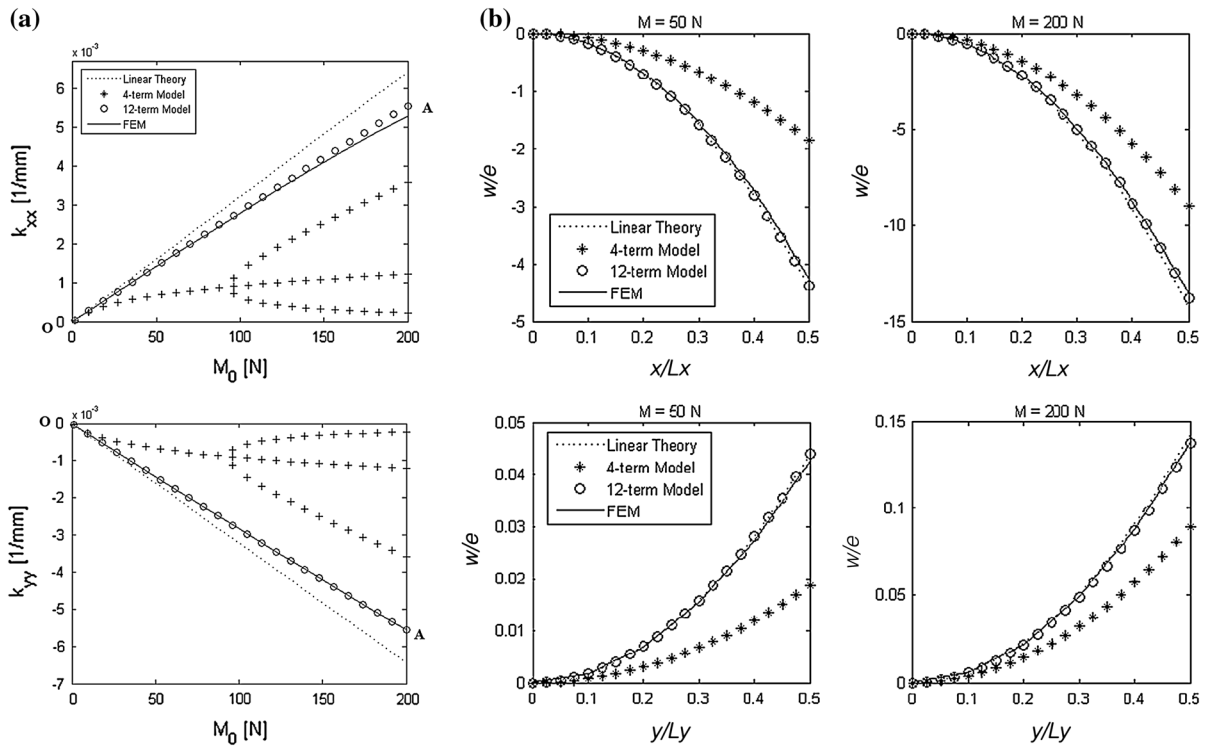
Fig. 6 a Longitudinal and transverse curvatures and **b** out-of-plane displacement as a function of the adimensional longitudinal (x/L_x) and transverse (y/L_y) coordinate for several values of the applied double bending moment ($M_{xx} = -M_{yy} = M_0$) for a rectangular isotropic plate (AR = 10)

Table 3 Orthotropic material properties for the double bending simulations

E_L	E_T	G_{LT}	v_{LT}
[GPa]	[GPa]	[GPa]	–
152	16.54	4.63	0.35

shape passes from square to rectangular, material, for plates whose constitutive behaviour splits from isotropic to orthotropic/anisotropic.

Figure 7 illustrates the *average* curvatures as a function of M_0 for an orthotropic square plate (AR = 1), as calculated by the linear (dotted line), the 4-term (cross points) and the 12-term (circles) models.

Both the 4-term and the 12-term models predict a loss of symmetric bifurcation behaviour which is coherent with the assigned level of orthotropy of the ply: a unique cylindrical-like shape has the tendency to develop with increasing M_0, while alternative solutions—among which one is unstable and not

observable (path C–D)—can be calculated starting from a given value of M_0 (point C in Fig. 7). Up to this point the predictions of the two models are in reasonably good agreement.

The situation is distinctly different for the case of an orthotropic heavily rectangular, narrow plate (AR = 10), illustrated in Fig. 8: the 4-term model keeps predicting loss of bifurcation behaviour qualitatively and quantitatively similar to the one plotted in Fig. 7, for a square plate, while the 12-term model a unique quasi-saddle shape tends to develop with increasing M_0. This solution is unique, for all values of M_0 in the explored range.

Again the finer discretisation put forward by the 12-term model—*which poorly contributes to the enhancement of the quality of the solution for square plates*—is *decisive* for the correct prediction of the multistable behaviour of rectangular—especially narrow—plates. This behaviour implies some considerations which will constitute—partly—the object of the next section.
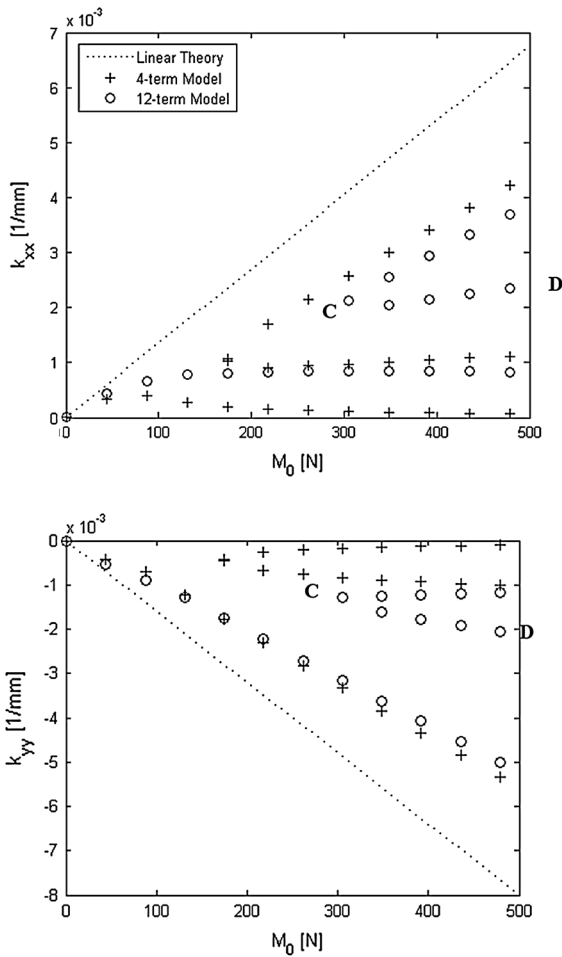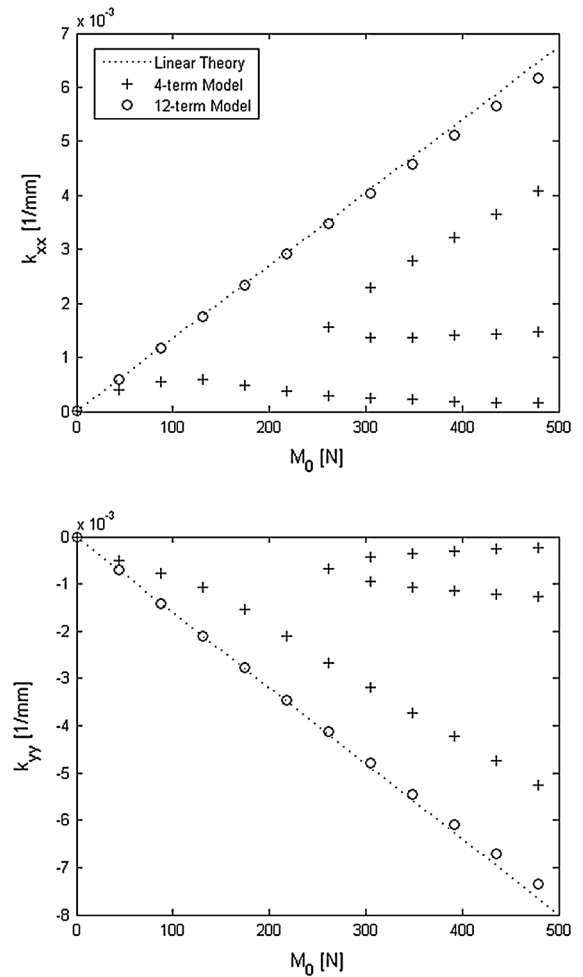
Fig. 7 Longitudinal and transverse curvatures as a function of the applied double bending moment ($M_{xx} = -M_{yy} = M_0$) for a square orthotropic plate ($E_T = 0.1E_L$, AR = 1)

Fig. 8 Longitudinal and transverse curvatures as a function of the applied double bending moment ($M_{xx} = -M_{yy} = M_0$) for a rectangular orthotropic plate ($E_T = 0.1E_L$, AR = 10)

3.3 Isotropic square and rectangular plates under nonlinear simple bending

The present section is devoted to the simulation of the behaviour of square and rectangular isotropic plates subjected to pure bending carried out by the 4-term and the 12-term nonlinear models as well as by the Ashwell's [22] analytical 'exact' solution. As a reference, the predictions of the Large Plate and of the Linear Plate (beam) Theory are also provided: the longitudinal and transverse curvatures according to the Linear theory are given, respectively, by

$$K_{xx} = \frac{M_0}{EI} \tag{50}$$

and

$$K_{yy} = -\nu K_{xx} \tag{51}$$

being EI is the flexural rigidity of the plate, while the Large Plate Theory is based on the assumption that the transverse curvature (along the y direction) is equal to zero, thus providing

$$K_{xx} = \frac{M_0}{EI}(1 - \nu^2) \tag{52}$$

$$K_{yy} = 0 \tag{53}$$

Ashwell 'exact' theory gives a nonlinear relationship between the applied bending moment, M_{xx}, and the resulting longitudinal curvature, that is

$$K_{xx} = \frac{M_0}{EI}\Phi \tag{54}$$

in which

$$\Phi = \frac{1}{1-v^2} + \frac{3}{2\alpha L_y}f(\alpha L_y) - \frac{2\sqrt{3}v}{\alpha L_y\sqrt{(1-v^2)}}F(\alpha L_y) \tag{55}$$

and

$$\begin{aligned}f(\alpha L_y) =\ &2(B^2 + C^2)(\sinh\alpha L_y + \sin\alpha L_y)\\&+ (B^2 - C^2 + 2BC)\cosh\alpha L_y\sin\alpha L_y\\&+ (B^2 - C^2 - 2BC)\sinh\alpha L_y\cos\alpha L_y\\&+ 2(B^2 - C^2)\alpha L_y\end{aligned} \tag{56}$$

$$\begin{aligned}F(\alpha L_y) = &(B + C)\sinh\frac{\alpha L_y}{2}\cos\frac{\alpha L_y}{2} - (B\\&- C)\cosh\frac{\alpha L_y}{2}\sin\frac{\alpha L_y}{2}\end{aligned} \tag{57}$$

B and C are expressed by Eqs. (19) and (20).

The aim of the present section is twofold:

– from one side, since no exact solution is available for the test cases presented in Sects. 3.1 and 3.2, a comparison with an analytical model helps strengthening the confidence about the employment of the developed models. This step is almost *an a posteriori validation* of the 12-term nonlinear model which is *in fact* built on a proper development of the Ashwell exact solution and therefore is expected to give comparable (if not identical) results,

– from the other side, and most importantly, this section tries to provide some proper discussion in support of the results presented in Sects. 3.1 and 3.2, in which it is seen that a modest/moderate refinement of the polynomial approximation *is in fact able to change dramatically the trend behaviour predicted by low-order polynomial models.*

Figure 9 shows the *average* longitudinal and transverse curvatures, K_{xx} and K_{yy}, as a function of M_0 for a square isotropic plate (AR = 1).

The 4-term, the 12-term and the Ashwell 'exact' theory predict the average longitudinal curvature with very good agreement, for all values of M_0: they are also in good agreement with the Large Plate Theory, leading to the conclusion that—with regard to simple bending behaviour—a square plate (AR = 1) can be considered as *Large* for all the tested values of M_0. Some small discrepancy can be observed between the approximate models (both the 4-term and the 12-term)

and the Ashwell 'exact' theory as soon as the prediction of the transverse curvature is concerned in particular for high values of M_0 ($M_0 > 300$ N). In order to elucidate the reason for such discrepancy, further investigation about the plate distortion is needed: to this aim Fig. 9b illustrates the adimensional out-of-plane displacements (w/e) as a function of the adimensional transverse coordinate, y/L_y, calculated at $x = 0$, for several values of the applied bending moment. While the 4-term model, which assumes constant curvatures, follows the Ashwell out-of-plane displacements only in average, the 12-term model follows closely the Ashwell exact theory, despite some small discrepancies for intermediate values of M_0. These discrepancies can be appreciated in the proximity of the external free edge ($y/L_y = 0,5$), where the 4-term and the 12-term models are not asked to satisfy exactly the boundary condition of zero transverse bending moment and are therefore *constrained* with respect to the development of a full anticlastic curvature.

Figure 10 shows the case of a moderately rectangular isotropic plate (AR = 4). The 12-term model and the Ashwell 'exact' theory both predict the average longitudinal and transverse curvatures with very good agreement, for all values of M_0, while the 4-term model fails predicting correctly the average transverse curvatures, differing significantly from the analytical solution: the discrepancy can be ascribed to the poor discretization of the displacement field which—for the 4-term model—is able to capture the deflection of the plate *only in average*, as illustrated in Fig. 10b.

Figure 11 illustrates the case of heavily rectangular 'narrow' plate (AR = 10). Here the behaviour predicted by the 4-term model differs distinctly from that calculated by the 12-term and by the 'exact' Ashwell model, which—as expected—are in excellent agreement for all values of M_0. But this is not all. The 12-term and the Ashwell 'exact' models are also in very agreement—almost surprisingly—with the Linear (beam) theory, for almost all the explored values of M_0: this behaviour can be appreciated by looking at the plots in Fig. 11b, illustrating the transverse deflection of the plate for several values of the applied bending moments. In this case the anticlastic curvature is less constrained than for square plates and can be well simulated by the 12-term distortion model: on the contrary, the 4-term model, which assumes constant
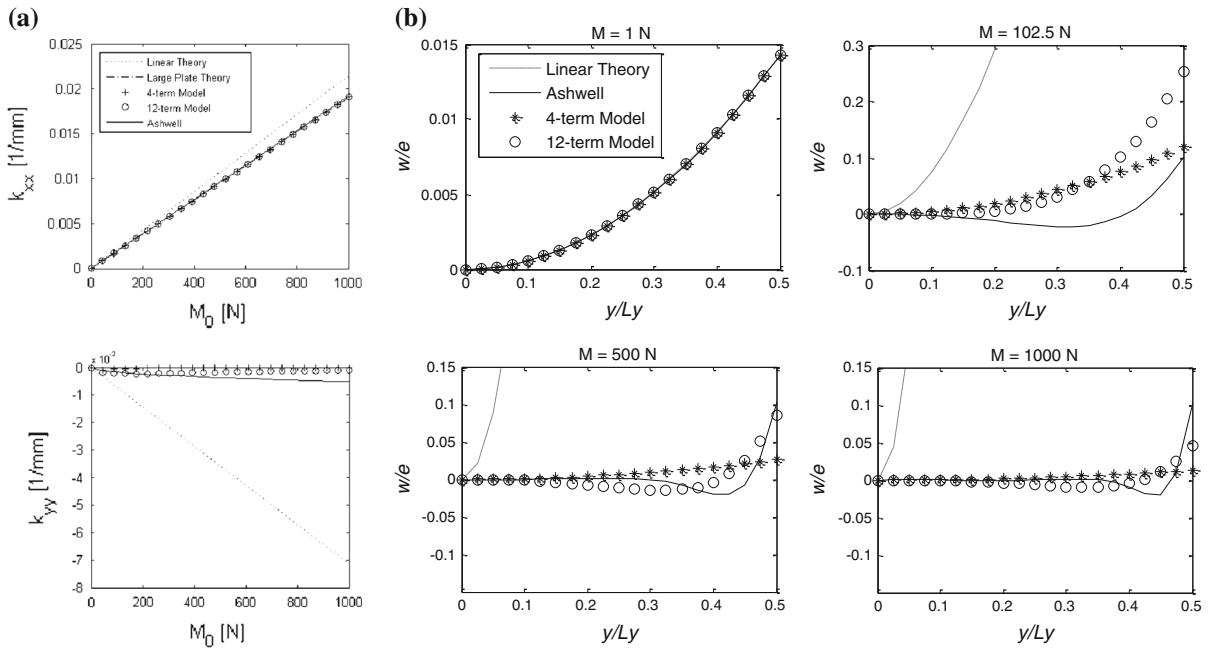
Fig. 9 **a** Longitudinal and transverse curvatures and **b** out-of-plane displacement as a function of the adimensional transverse coordinate (y/L_y) for several values of the applied bending moment ($M_{xx} = M_0$) for a square isotropic plate (AR = 1)
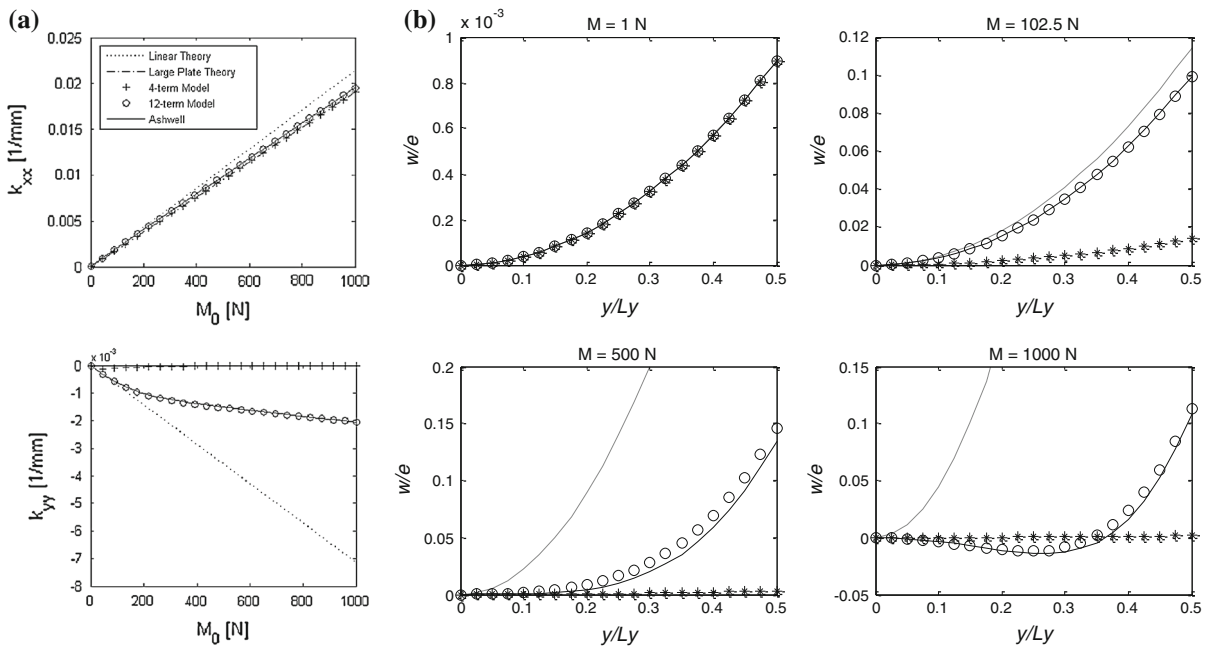
Fig. 10 **a** Longitudinal and transverse curvatures and **b** out-of-plane displacement as a function of the adimensional transverse coordinate(y/L_y) for several values of the applied bending moment ($M_{xx} = M_0$) for a rectangular isotropic plate (AR = 4)

(a)

(b)
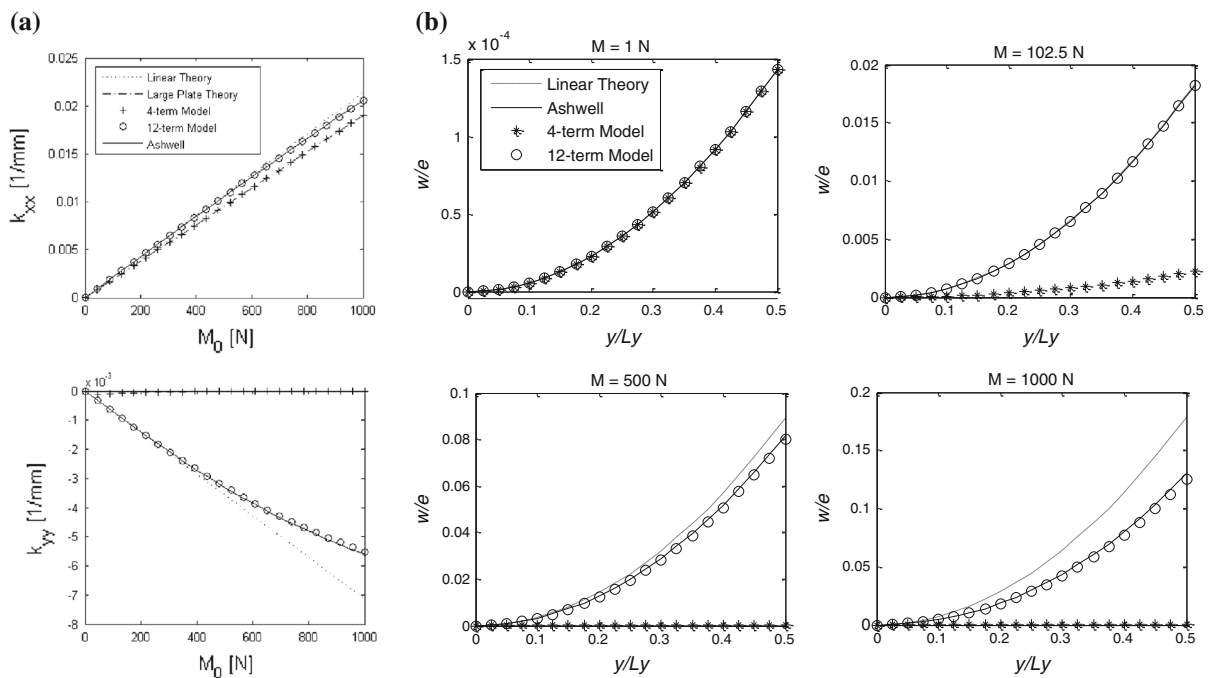
Fig. 11 a Longitudinal and transverse curvatures and **b** out-of-plane displacement as a function of the adimensional transverse coordinate (y/L_y) for several values of the applied bending moment ($M_{xx} = M_0$) for a rectangular isotropic plate (AR = 10)

curvatures, is evidently too stiff with respect to the 'exact' theory and keeps following closely the predictions of the Large Plate model—still for narrow plates.

This result suggests an almost unexpected conclusion: *with regard to simple bending behaviour a heavily rectangular 'narrow' plate can be considered as a beam in a large loading range.*

Going further along this line of reasoning it can be concluded that the Linear (beam) and the Large Plate Theories represent two sort of bounds incorporating all the explored structural solutions: the bending behaviour is characterised by 'large plate-to-beam' transition which occurs when switching from square to heavily rectangular plate configuration and *ruled by the mode of distortion of such configurations.* This phenomenon *results in a dramatic change of the apparent bending stiffness of the plates* and *affects their response with respect to an externally applied bending load.* Ashwell had already noted this result and indicated the main parameter affecting the bending behaviour: *this parameter* (*see Eq.* 21)—*deciding the mode of distortion*—*depends mainly on the plate width* (*"breadth" in Ashwell's words*).

The above reasoning provides some motivation for discussing the results presented in Sect. 3.1 and 3.2

about square and rectangular plates subjected to distributed bending moments of equal magnitude and opposite sign along two orthogonal directions. This discussion can be roughly summarised as follows: though the bending moments are nominally of equal magnitude, the apparent stiffness across the two orthogonal directions is not the same—except for square plates—and is affected by the breadth measured along that direction. Therefore—though the rectangular configuration is symmetrical from the point of view of loading—*it is not* from the point of view of the apparent stiffness, leading to a loss of symmetry of its global structural response. The perfect symmetric configuration—from all viewpoints—is represented by the square one: as soon as this configuration is abandoned *plate-to-beam transition takes plates and symmetry is lost.* A polynomial model trying to reproduce such behaviour must be sufficiently rich to reproduce—though approximately—*at least* plate-to-beam transition: in the present context, among the explored discretisation functions, it is evident that the 4-term model is too stiff to simulate this transition correctly and works badly with rectangular plates, while the 12-term model is *sufficiently* rich to handle this condition.

Table 4 Relative simulation times

Linear Theory	4-term model	12-terms model
0.33	1	7

By the above results the following conclusion can be tentatively extrapolated: since the 4-term Hyer's model [25] has been already successfully applied for the prediction of the cured shape of square composite plates under thermal loads, it is reasonable to think that the 12-term model has some chance to work satisfactorily for predicting the distortion of square *and* rectangular plates under thermal loads, temperature gradients and for more complex multi-physical applications. Future research is needed to set this set of conclusions on more solid grounds.

As a conclusion, Table 4 presents the difference between the simulation times of the different models, taking as 1 the simulation time of the 4-term model. The Linear theory is around three times faster than the 4-term model, which is geometrically nonlinear. The 12-term model is only 7 times slower than 4-term model, giving more affordable results.

4 Conclusion

The paper presents an efficient 12-term Rayleigh–Ritz based model to predict *the deformed shape of isotropic and orthotropic square and rectangular plates subjected to double bending loads distributed along all edges within the framework of the nonlinear Von Karman theory*: this investigation may serve as a basic reference test case for more complex structural conditions (multistable plates and shells…). The out-of-plane and in-plane displacement functions of the model are generated through proper development of the analytical solution proposed by Ashwell [22] for the pure nonlinear bending of plates and of the semi-analytical expression of strain proposed by Galletly and Guest [28] for the nonlinear deformation of slit tubes. The model is characterised by high-order displacement functions and by few unknown terms and it is therefore appropriate to achieve sufficient accuracy, with high efficiency.

The performance of the model is tested against the 4-term model by Hyer [25]—a low-order/low-parameter approximation characterised by uniform curvatures across the plate—the finite element model and the Ashwell [22] analytical solution for the nonlinear simple bending of isotropic plates.

The lack of an analytical explicit expression for the critical bifurcation bending load for isotropic and anisotropic plates subjected to double bending moment does not help does not help deciding in favour of one of the two approximated displacement fields, for square plates (AR = 1). However, with respect to the 4-term model, the 12-term model is capable to capture with sufficient accuracy the loss of symmetric bifurcation phenomena occurring in rectangular isotropic and orthotropic plates under double bending moments.

As discussed in Sect. 3.3 these phenomena are strictly related to the large plate-to-beam transition effect occurring in rectangular plate configurations when switching from low to high Aspect Ratio values: the 12-term approximation is sufficiently accurate to catch this transition satisfactorily.

In future research experimental validation of the predicted features will be provided: moreover the model will be applied for the simulation of more complex situations, involving for instance plates and shells subjected to the effect of multi-physical coupled solicitations, temperature gradients, nonuniform solvent distribution, electro-mechanical load…

References

1. Timoshenko S (1925) Analysis of bi-metal thermostats. J Opt Soc Am 11:233–255
2. Hyer MW (1981) Some observations on the cured shapes of thin unsymmetric laminates. J Compos Mater 15:175–194
3. Kim KS, Hahn HT (1989) Residual stress development during processing of graphite/epoxy composites. Compos Sci Technol 36:121
4. Jun JW, Hong CS (1992) Cured shape of unsymmetric laminates with arbitrary lay-up angles. J Reinf Plast Compos 2:1352–1366
5. White SR, Hahn HT (1992) Process modelling of composite materials: residual stress development during cure. Part II: experimental validation. J Compos Mater 26:2423
6. Sarrazin H, Kim B, Ahn SH, Springer GS (1995) Effect of processing temperature and layup on springback. J Compos Mater 10:1278
7. Cowley KD, Beaumont PWR (1997) The measurement and prediction of residual stresses in carbon-fibre/polymer composites. Compos Sci Technol 57:1445–1455

8. Tarsha-Kurdi KE, Olivier P (2002) Thermoviscoelastic analysis of residual curing stresses and the influence of autoclave pressure on these stresses in carbon/epoxy laminates. Compos Sci Technol 62:559–565

9. Gigliotti M, Wisnom MR, Potter KD (2003) Development of curvature during the cure of AS4/8552 0/90 unsymmetric composite plates. Compos Sci Technol 63:187

10. Gigliotti M, Molimard J, Jacquemin F, Vautrin A (2006) On the nonlinear deformations of thin unsymmetric 0/90 composite plates under hygrothermal loads. Compos A Appl Sci Manuf 37:624–629

11. Gigliotti M, Jacquemin F, Molimard J, Vautrin A (2007) Transient and cyclical hygrothermoelastic stress in laminated composite plates. Modelling and experimental assessment. Mech Mater 39:729–745

12. Hufenbach W, Gude M, Kroll L (2002) Design of multistable composites for application in adaptive structures. Compos Sci Technol 62:2201–2207

13. Aimmanee S, Hyer MW (2004) Analysis of the manufactured shape of rectangular THUNDER-type actuators. Smart Mater Struct 13:1389–1406

14. Aimmanee S, Hyer MW (2006) A comparison of the deformations of various piezoceramic actuators. J Intell Mater Syst Struct 17:167–186

15. Seffen KA (2007) 'Morphing' bistable orthotropic elliptical shallow shells. Proc R Soc A 463:67–83

16. Mattioni F, Gatto A, Weaver PM, Friswell MI, Potter KD (2006) The application of residual stress tailoring of snap-through composites for variable sweep wings. In: 47th AIAA/ASME/ASCE/AHS/ASC structures, structural dynamics and materials conference (1972), Newport

17. Diaconu CG, Weaver PM, Mattioni F (2008) Concepts for morphing airfoil sections using bi-stable laminated composite structures. Thin-Walled Struct 46:689–701

18. Mattioni F, Weaver PM, Friswell MI (2009) Multistable composite plates with piecewise variation of lay-up in the planform. Int J Solids Struct 46:151–164

19. Fernandes A, Maurini C, Vidoli S (2010) Multiparameter actuation for shape control of bistable composite plates. Int J Solid Struct 47:1449–1458

20. Pirrera A, Avitabile D, Weaver PM (2010) Bistable plates for morphing structures: a refined analytical approach with high-order polynomials. Int J Solids Struct 47:3412–3425

21. Forterre Y, Skotheim JM, Dumais J, Mahadevan L (2005) How the venus flytrap snaps. Nature 433:421–425

22. Ashwell DG (1950) The anticlastic curvature of rectangular beams and plates. J R Aeronaut Soc 54:780

23. Pao YC (1970) Simple bending analysis of laminated plates by large-deflection theory. J Compos Mater 4:380–389

24. Hyer MW, Bhavani PC (1984) Suppression of anticlastic curvature in isotropic and composite plates. Int J Solids Struct 20:553–570

25. Hyer MW (1981) Calculation of the room-temperature shapes of unsymmetric laminates. J Compos Mater 15:296–310

26. Vidoli S (2013) Discrete approximations of the Föppl-Von Kármán shell model: from coarse to more refined models. Int J Solids Struct 50:1241–1252

27. Timoshenko S, Woinowsky-Krieger S (1959) Theory of plates and shells, 2nd edn. McGraw-Hill, New York

28. Galletly DA, Guest SD (2004) Bistable composite slit tubes. I. A beam model. Int J Solid Struct 41:4517–4533

29. Herakovich CT (2012) Mechanics of composites: a historical review. Mech Res Commun 41:1–20